Int. J. of Thermal & Environmental Engineering
Volume 20, No. 1 (2023) 21-28

Optimizing Gas Turbine Performance: Influence of Angle of Attack and Mist Cooling

Omar Nasro, Said ELTurk, Isam Janajreh*

Department of Mechanical Engineering, Khalifa University of Science and Technology, Abu Dhabi, UAE

Abstract

This work presents a comparative study of the flow over a gas turbine blade aimed at enhancing turbine performance. The study focuses on determining the optimal angle of attack of the fluid and implementing internal turbine blade cooling. Computational Fluid Dynamics (CFD) was employed under varying parameters, including fixed and rotating turbine blade conditions. Precise analysis of temperature and pressure coefficient distributions, as well as torque, enthalpy, thermodynamic power, flow velocity, and mass flow rate were conducted for each setup. Results indicate that the optimal flow attack angle is 60°. Subsequently, mist cooling was simulated as an internal cooling method at the optimum attack angle to examine its effect on blade temperature distribution. Simulation outcomes suggest that implementing mist cooling enhances temperature distribution over the blade and improves turbine performance.

Keywords: *Turbine Blades, Turbine Cooling, Gas Turbine, Internal Cooling, Mist Cooling, CFD.*

1. Introduction

The Brayton cycle has been broadly used due to its dependability and durability as a significant power source for a long time. Increasing the efficiency of gas turbines that operate on Brayton cycles has always been a desirable topic for engineers. In this study, two methods will be investigated in order to increase the gas turbine's performance. Firstly, finding the best fluid attack angle. Secondly, integrating the blade cooling method will allow the increase of the cycle's limit temperature. Where according to the Carnot efficiency, the maximum theoretical efficiency of gas cycles (upper limit of the efficiency) is dependent on the ratio of the lowest temperature in the cycle to the highest temperature in the cycle, as shown in Equation 1 [1]. However, the turbine's safety should also be taken into consideration to protect the turbine blades from high-temperature streaks, and, consequently, thermal stresses, high oxidation rates, and short creep life, which might occur if the highest cycle temperature increases beyond a specific range [1]. The progress of enhancing the energy output of blades owes much to developments in metallurgical science, particularly in the materials employed within gas turbines [2]. Turbines can take a maximum temperature of approximately 1500°C – 1700°C. Hence, the local temperature of a turbine blade must be reduced. Moreover, Reyhani et al. [3] explored the impact of hot section component durability on the operational costs of modern gas turbines. They highlighted that certain defects may arise, which have the potential to reduce the lifespan of turbine blades within the hot section. Hence, they presented methods used for calculating blade temperature and life. A well-known effective method that will be tested to do so is the Closed Loop Misting. Closed loop misting is simply injecting mist into the fluid flow before entering the turbine [4]. Mist consists mainly of droplets of water that play the role of a heat sink, whereas the droplets tend to evaporate by scavenging and on the high temperature thermal streak for their latent heat and reducing its temperature before reaching the turbine blades [4]. The water droplets travel for some distance through the fluid before vaporizing completely. When using closed loop misting cooling, the process can be controlled by adjusting the size (diameter) of the droplets that are being injected into the fluid flow [4]. That is because the temperature decreases not only by the droplets' evaporation but also because of the specific heat of the injected water, which is larger for droplets with larger diameters [4]. Li and Wang [5] proposed that a small amount of mist injection could enhance the results of power generated and increase the adiabatic film cooling efficiency by around 30% to 50%. In addition, 2% of the coolant mass flow rate is enough to enhance efficiency [5]. Moreover, they found that mist cooling was less efficient for cases of low pressure and temperature conditions [6]. Dhanasekaran et al. [7] successfully improved the efficiency of turbine blades computationally by simulating misting behavior. Moreover, other simulations done by Jiang et al. [8] found that mist cooling effectively reduces the temperature of the boundary

* Corresponding author. Tel.: +971 2 312 3286
E-mail: Isam.Janajreh@ku.ac.ae

DOI: 10.5383/ijtee.20.01.004

layer without affecting the temperature of the mainstream flow or the thickness of the boundary layer. Additionally, they noted that laboratory experiments have demonstrated that injecting mist into the cooling fluid can enhance cooling effectiveness by 50% to 800%.

Another method related to misting is the injection of high-pressure inlet fogging, which is a method that converts the demineralized water into fog droplets as a cooling method of the inlet air in the blades [9]. Chaker et al. [11] presented comprehensive experimental and theoretical research, with insights gained from implementing over 400 inlet fogging systems on gas turbines. Previous research has proven that the effectiveness of such a cooling system can be influenced by other factors, such as the rotation of a rotating gas turbine, where the effectiveness of the cooling system decreases with increasing rotation [1]. Barakat et al. [12] introduced new hybrid cooling systems and compared it with other configurations of gas turbine systems. They developed three models: one predicted fogging system cooling potential, another analyzed earth-air heat exchanger thermal behavior, and a third combined both systems into a hybrid cooling setup. Comparing these techniques at the New Damietta power plant in Egypt, the hybrid system proved superior, boosting average annual energy by 9.8% compared to 8% and 6.6% for fogging and earth-air heat exchanger systems, respectively. Another research found this closed-loop cooling method to successfully increase the efficiency of a gas cycle by up to 60% [1].

There are more methods for enhancing gas turbine efficiency, that are divided into different categories such as: Evaporating cooling [13], absorption chiller cooling [14], refrigeration cooling [15], and thermal energy storage [16].

$$maximum\ theoretical\ efficiency = 1 - \frac{T_L}{T_H} \quad (1)$$

The simplest definition of the angle of attack (AoA) for a two-dimensional blade, is the geometrical angle between the flow direction and the cord line of the blade [10]. Changing of the stator angle, which implies changing the AoA for turbine rotor in complete turbine stage can lead to a significant effect on the distribution of the pressure and the suction sides of the turbine's blades [17]. This adjustment of the AoA can affect directly the power extracted from the flow by the turbine, particularly the specific power (defined as the ratio of shaft power to the mass flow rate). The tangential and radial flow velocities are modified by changing the flow angle. The preceding discussion underscores the significance of investigating flow angle sensitivity to determine the optimal AoA for the rotor inlet, a task facilitated by integrating stator blades. Furthermore, it emphasizes the importance of attaining precise and varied flow patterns necessary for implementing misting techniques to study their impact on blade cooling.

The organization of this work is as follows: The methodology is explained in the next section along with the geometry setup and mesh sensitivity study. The results are presented in the following section. Conclusions and recommendations are drawn up at the end.

2. Methodology

Fig. 1 represents the turbine's rotor geometry which is developed using the Gambit Turbo tool. The turbine domain is constructed by providing: (i) several cross-sections of the blades (minimum two) starting from the hub at the root and ending near the casing, (ii) additional to two lines representing the hub and the casing axes around a specified coordinate reference (typically the x-axis), and (iii) the number of the rotor blades. Geometry is created by radial surface sweeping of the blade cross-sections and the two surfaces of revolution made by the hub and casing lines that divide the domain into equal rotational periodic segments specified by the number of blades. This creates one rotor segment domain/volume bounded by six surfaces. These are the hub and casing wall surfaces, upstream inlet, and downstream outlet regions normal to the turbine's axial planes, and two periodic surfaces of similar topography. The blade's surface walls are identified as pressure and suction blade surfaces. The domain can be considered fixed or rotating reference frame (RRF) simulating fixed or rotating rotor, respectively. The RRF is governed by the fluid flow governing equations that are for rotating frame (steadily) representing the conservation of mass (Eq. 2a), momentum (Eq. 3a), and energy (Eq. 4a). The flow is governed by the compressible Navier-Stokes equations for turbulent flow regime representing the conservations of mass (Eq. 2b), momentum (Eq. 3b), and energy (Eq. 4b) as:

$$\frac{\partial \rho}{\partial t} + \frac{\partial}{\partial x_i}(\rho \overrightarrow{v_r}) = 0 \quad (2a)$$

$$\frac{\partial}{\partial t}(\rho \vec{v}) + \frac{\partial}{\partial x_j}(\rho \overrightarrow{v_r} \vec{v}) + \rho(\overrightarrow{\omega_r} \times \vec{v}) = -\frac{\partial P}{\partial x_i} + \frac{\partial \tau_{ji}}{\partial x_j} + \vec{F} \quad (3a)$$

$$\frac{\partial}{\partial t}(\rho e) + \frac{\partial(\rho \overrightarrow{v_r} H + \rho \overrightarrow{u_r})}{\partial x_i} = \frac{\partial}{\partial x_j}\left[k \nabla T + \tau_{ji} \rho\right] + S_h \quad (4a)$$

$$\frac{\partial \rho}{\partial t} + \frac{\partial}{\partial x_i}(\rho v_i) = 0 \quad (2b)$$

$$\frac{\partial}{\partial t}(\rho v_i) + \frac{\partial}{\partial x_j}(\rho v_i v_j) = -\frac{\partial P}{\partial x_i} + \frac{\partial \tau_{ji}}{\partial x_j} + \rho g_i \quad (3b)$$

$$\frac{\partial}{\partial t}(\rho e) + \frac{\partial \rho e v_j}{\partial x_i} = \dot{q} + \frac{\partial \dot{q}}{\partial x_i} + \frac{\partial}{\partial x_j}[(-\rho \delta_{ij} + \tau_{ji}) v_i] + \rho g_i v_i \quad (4b)$$

Turbomachinery equations that govern the energy extracted by the turbine kinematically is written as:

$$\frac{P_s}{\dot{m}} = U_{in} V_{u\,in} - U_{out} V_{u\,out} \quad (5)$$

Eq. 5 can be further simplified by assuming a negligible value for $V_{u\,out}$, denoted as:

$$\frac{P_s}{\dot{m}} = U_{in} V_{u\,in} \quad (6)$$

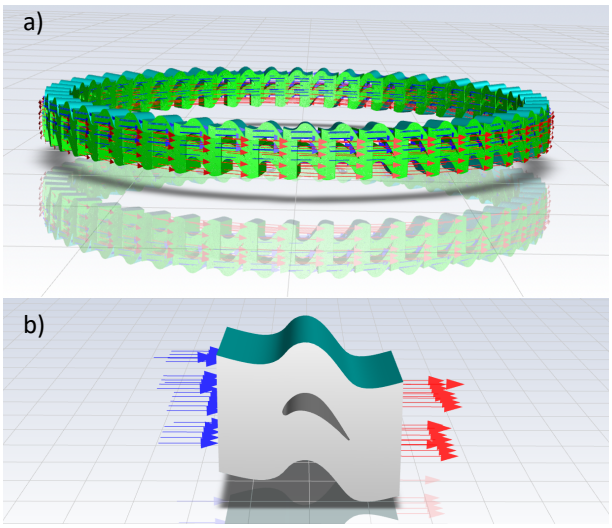

Fig. 1: Construction of the model for a 50-blade rotor: (a) the entire domain, and (b) the periodic domain segment

Fig. 1(a) shows the constructed turbine rotor that comprises of 50 blades separated circumferentially at an angle of 5.0 degrees between two consecutive blades. The extracted domain in Fig. 1(b) from the complete rotor in Fig. 1a extends in the x-direction from -0.015 m to 0.042 m, in the y-direction from -0.035 m to 0.027 m, and in the z-direction 0.298 m to 0.330 m. It is subjected to a total pressure, flow direction and prescribed temperature at the inlet (blue arrows) while a prescribed static pressure at the outlet. All walls are prescribed with no slip kinetically and adiabatic thermally.

The designed blade has a cord length of 1.6 cm, cord width of 0.32 cm, maximum width position near 30% of the cord, i.e., 0.48 cm from the blade leading edge, and a maximum camber of 0.50 with nearly 250 twists from the root until the casing. Fig. 1 shows the domain segment where the oriented top and bottom surfaces are designated with periodic boundaries, which means that no flow passes through them. Also, since they are periodic boundaries, they are connected, which means that a single point on the top surface will correspond to the same point on the bottom surface. The usage of this model enables one to study the flow attack angle, and hence proper integration of the stator to guide the flow as well inclusion of misting along with the incoming flow to the rotor.

The mesh for this model is generated using Gambit, employing a hexagonal mesh that incorporates surface boundary layers at the blade, hub, and casing surfaces, with an initial cell height of 0.1mm, an inflation ratio of 1.2, and consisting of 10 rows. The baseline mesh comprises 918,000 nodes, with Fig. 2 illustrating the meshing depicting the boundary layer around the pressure and suction surfaces of the blade. This approach ensures precise capturing of the flow gradient, crucial for accurately evaluating energy transfer and torque at the blade surface. The rotor is considered firstly at zero rpm and then at 5,000 rpm.

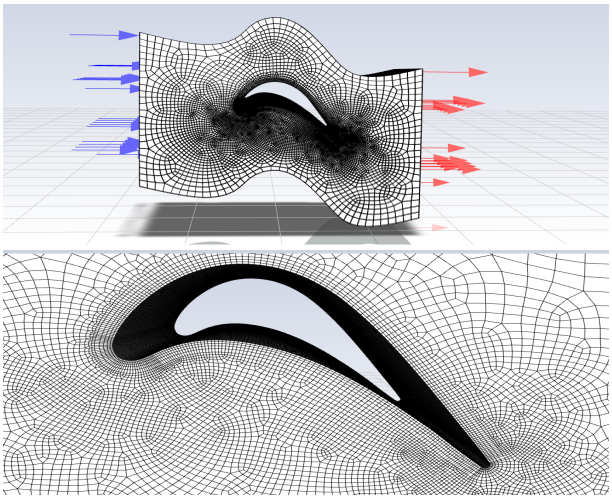

Fig. 2: The mesh utilized in the simulations, with a close-up view near the blade illustrating the inflation of the boundary layer

The fluid flowing around the blade is assumed to be hot air behaving as an ideal gas, but with fixed specific heat, thermal conductivity, viscosity, and molecular weight of 1006.43 J/kg K, 0.0242 W/m-K, 1.7894e-05 kg/m-s, and 28.966 kg/kg/kmol, respectively. The blade is considered to be made of nickel chrome alloy with a density of 2719 kg/m^3, a specific heat of 871 J/kg-K, and thermal conductivity of 202.4 W/m-K. AoA is changed by controlling the incoming axial and circumferential components of the flow. These angles are set at 0° (axial), 40°, 50°, 60°, and 70°. The selection of these angles is due to the fact that the guiding vanes in practical gas turbines usually guide the flow at angles in the range of 35°-70°. For example, the angle of 40° was set by using the following calculation:

$$tan\left(\frac{V_y}{V_x}\right) = 40° \rightarrow V_y = \tan^{-1}(40) \times V_x = \tan^{-1}(40°) \times 1 = 0.839099631\,\frac{m}{s}$$

All angles were taken with respect to the positive x-axis.

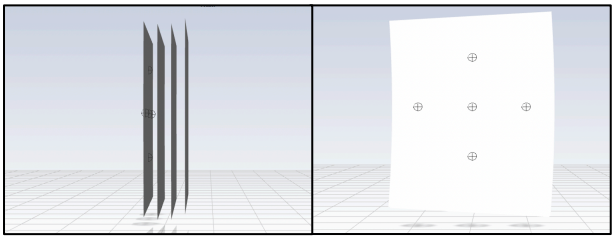

Fig. 3: Flow crossing planes at the upstream and mist injection points on the first plane

As for the misting integration, four vertical surface planes were created at the front of the blade's leading edge, as shown in Fig. 3. This is to observe the injection of the droplets and the temperature distribution that will result from the injection. The planes have a fixed distance of 0.003 m between each other, where the first plane has an axial shift with coordinates (-0.001,0,0), and the last plane has coordinates (-0.01,0,0). The mist injection was done through five points on the first plane, as shown in Fig. 3. The points have coordinates of (-0.001, 0, 0,315), (-0.001, 0, 0.325), (-0.001,0,0.305), (-0.001, -0.01,0.315), and (-0.001,0,0).

Moreover, the flow rate of the liquid water droplets was approximately 0.1% of the flow rate of the air, and the diameter of the droplet and its temperature were set at 0.1 mm and 300 K, respectively.

Table 1: Summary of reference values

Property	Value
Area - A_o (m^2)	0.0009
Density - $\rho_o(kg/m^3)$	1.225
Enthalpy - $h_o(J/kg)$	0
Length - $L_o(m)$	0.03
Pressure - $P_o(bar)$	0
Temperature - $T_o(K)$	288.16
Viscosity - $\mu_o(kg/m\ s)$	1.79E-05
Ratio Of Specific Heats	1.4

Table 1 outlines the reference values established for various parameters, maintained consistently across all simulations to ensure a fair and valid comparison between different runs. Table 2 provides a summary of the boundary conditions for each run, encompassing inlet and outlet temperatures, velocity components, pressures, and rotation speed. For each case, key metrics such as pressure distribution, temperature distribution, pressure coefficient distribution, torque, enthalpy, thermodynamic power, energy, flow velocity, and mass flow rate were calculated and analyzed. Additionally, simulations were conducted at zero rotation to establish a baseline, crucial for comparative analysis across different angles.

Table 2: Summary of the boundary conditions

θ (°)	V_0 (m/s)	T_{in} (K)	T_{out} (K)	$P_{in\ (total)}$ (bar)	$P_{out\ (static)}$ (bar)	ω (rpm)
0	1	1500	1200	22.8	13.6	5000
40	259.3	1500	1200	22.8	13.6	5000
50	334.4	1500	1200	22.8	13.6	5000
60	385.0	1500	1200	22.8	13.6	5000
70	468.9	1500	1200	22.8	13.6	5000

3. Results and Discussion

To determine the optimal AoA, the total torque generated by the blade surface (comprising both suction and pressure sides) is monitored, along with the mechanical power calculated as the product of the total torque and rotor angular speed. The optimal Angle of Attack (AoA) should result in the highest torque exerted by both the suction and pressure sides of the blade. As mentioned earlier, adjustments in the vertical velocity are utilized to modify the attack angle of the flowing fluid. Fig. 4 and Fig. 5 illustrate the temperature and pressure coefficient distributions obtained at the middle radial plane of the simulated flow domain segments for input flow directions of 40 and 60 degrees. Additionally, metrics such as inlet mass flow rate, inlet and outlet mass-averaged enthalpies, and blade torque (from both suction and pressure sides) were recorded. Further analysis included calculations of total power, thermodynamic power, energy, mechanical power, and percentage error for each angle.

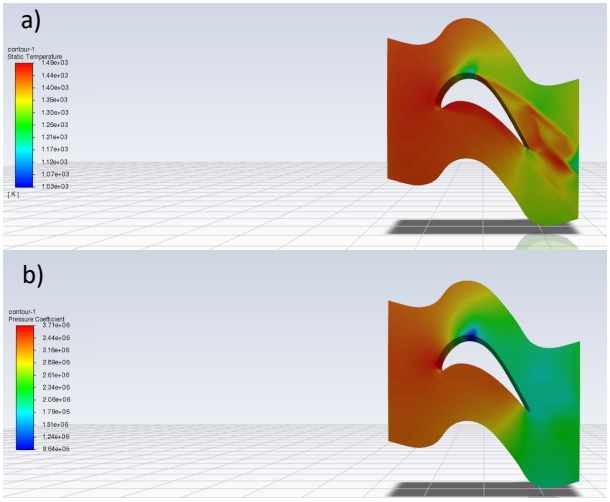

Fig. 4: a) The distributions of total temperature b) and pressure coefficient at an Angle of Attack (AoA) of 40°

At a flow angle of 40 degrees, as depicted in Fig. 4, it is evident that the high temperature at the inlet extends to the leading edge of the blade and remains elevated on the pressure side more than on the suction side. This occurrence can be attributed to direct exposure to the hot gas from the inlet section. The temperature gradually decreases near the suction side, whereas it remains relatively constant near the pressure side. Fig. 4 also illustrates the pressure coefficient distribution, representing the ratio of forces caused by pressure to those due to inertia. This distribution closely mirrors the trend observed in the temperature distribution. Notably, the pressure coefficient is higher on the pressure side compared to the suction side, which is advantageous as it facilitates easier blade rotation, leading to increased power production. Additionally, it is observed that the decrease in the pressure coefficient near the suction side is more pronounced compared to the temperature distribution.

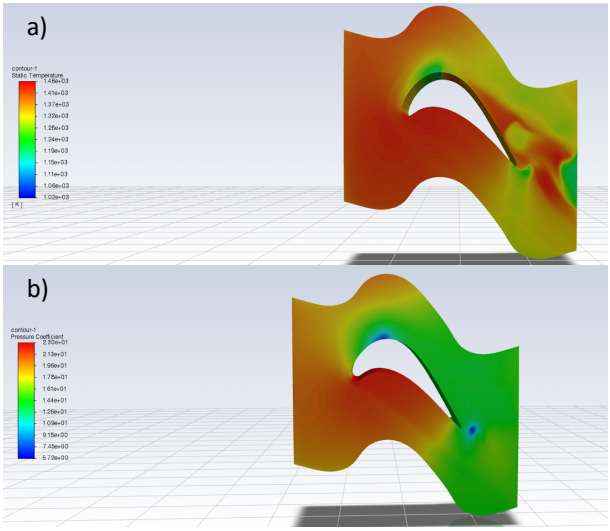

Fig. 5: The distributions of a) total temperature b) and pressure coefficient (bottom) at an Angle of Attack (AoA) of 60°

Fig. 5 illustrates the temperature and pressure coefficient distributions across the blade at an AoA of 60°. It exhibits a similar trend to that observed at an AoA of 40°, albeit with notably lower pressure coefficient values. As before, the pressure coefficient on the suction side surpasses that on the pressure side. Further analysis of the obtained flow variables is conducted utilizing the power equations as follows:

$$Power_{Thermodyanmics} = \dot{m}(h_{in} - h_{out}) \quad (7)$$

$$Power_{\ Mechanical} = torque\ total\ \times \omega\ \times \frac{2\pi}{60} \quad (8)$$

$$Total\ \ power = Power\ per\ blade\ \times number\ of\ blades \quad (9)$$

$$Total\ mechanical\ power = Mechanical\ power\ per\ blade\ \times number\ of\ blades \quad (10)$$

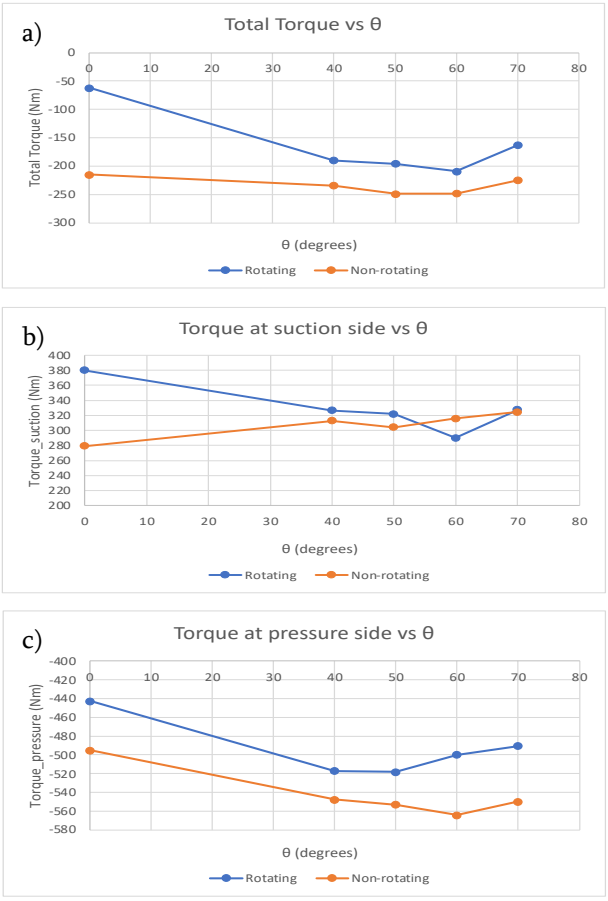

Fig. 6: Variation of: a) total torque, b) torque at the suction side, and c) torque at the pressure side, with respect to the Angle of Attack (AoA)

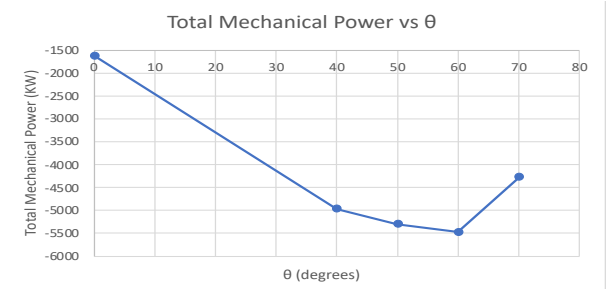

Fig. 7: Total Mechanical Power Output vs Angle of Attack

The results from the rotating model reveal a loss in mass flow rate between the inlet and outlet, expected due to flow blockage caused by blade curvature despite the system being closed. Fig. 6(a) depicts the trend of total torque, which increases until reaching a peak at AoA=60° (-209.1 Nm) before decreasing. Similarly, torque at the suction side, shown in Fig. 6(b), decreases until reaching a minimum at AoA=60° (290.2 Nm) before increasing again. Fig. 6(c) illustrates the behavior of torque at the pressure side, increasing until reaching a peak at AoA=50° (-583.3 Nm) before decreasing. Furthermore, Fig. 7 demonstrates that total mechanical power increases with increasing AoA, reaching a maximum of -5472.7 kW at AoA=60° before declining. Based on these observations, an AoA of 60° is deemed optimal, as it yields the maximum mechanical power output, the lowest torque on the suction side, and the maximum total torque. Although the torque on the pressure side is higher at AoA=50°, the marginal difference between the two values pales in comparison to the advantages offered by AoA=60° across other parameters. After determining the best AoA, the mist cooling method is simulated with the same model using 60° as an AoA.

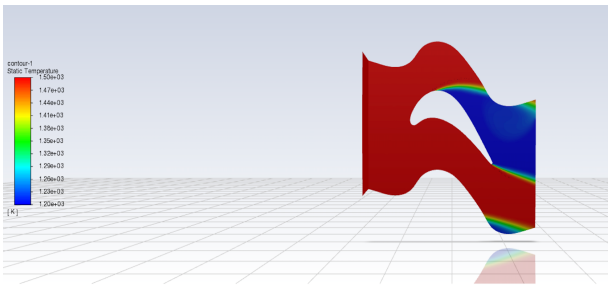

Fig. 8: Misted temperature distribution (AoA=60°)

Fig. 8 displays the temperature distribution along the blade when employing mist cooling. A comparison between Fig. 8 and Fig. 5 indicates the successful application of the cooling method in safeguarding the turbine blade. Significantly, a large portion of the blade is exposed to much lower temperatures compared to the scenario without misting. Consequently, this reduction in thermal stress contributes to less wear and tear on the blade. Moreover, the total torque of the blade measures -220.5 Nm, resulting in a total turbine power output of -5770.2 kW, surpassing the turbine power output at the same AoA without misting. This underscores the efficiency of the mist cooling method in enhancing turbine performance.

An additional five simulations were conducted within the baseline model to determine the optimal AoA that yields the highest torque. As outlined in the methodology section, each simulation aims to identify the most favorable AoA by assessing the specified properties. Fig. 9(a) depicts the static temperature distribution for the baseline model at an AoA of 40°. While the static temperature distribution for the baseline model mirrors that of the main model. There are notable distinctions, such as the temperature at the trailing edge, which, in this case, exhibits a lower temperature compared to the main model. This variance can be attributed to the non-rotating feature applied in the baseline model.

Furthermore, Fig. 9(b) illustrates the pressure coefficient distribution on the pressure side, suction side, and within the blade interior at an AoA of 40°. The pressure coefficient distribution exhibits nearly identical behavior in both the rotating and non-rotating cases. However, at the trailing edge, the pressure coefficient is higher in the non-rotating case. On the pressure side, the pressure coefficient surpasses that of the suction side, attributed to the downward direction of the flow, which is below horizontal.

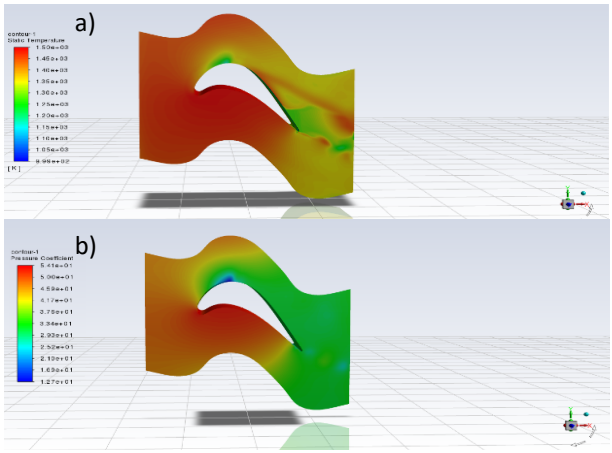

Fig. 9: The distributions of total a) temperature b) and pressure coefficient at an Angle of Attack (AoA) of 40°

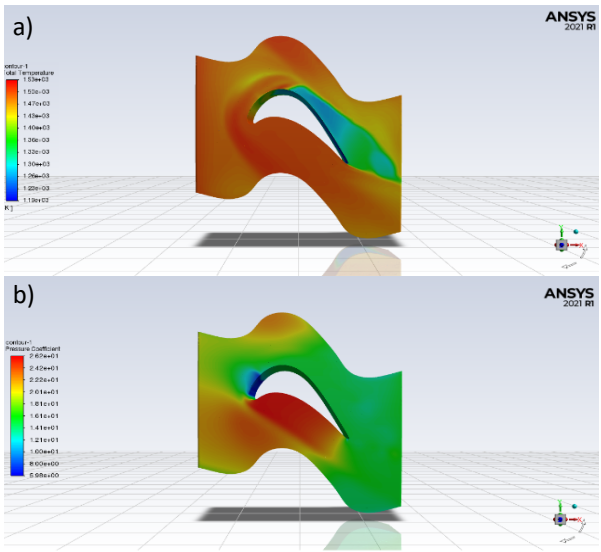

Fig. 10: The distributions of total temperature (top) and pressure coefficient (bottom) at an Angle of Attack (AoA) of 60°

Fig. 10(a) presents the total temperature on the baseline model. Meanwhile, Fig. 10(b) displays the pressure coefficient distribution at an AoA of 60°. Notably, this figure demonstrates improved results on the pressure side, with a clear increase in the pressure coefficient and a corresponding decrease on the suction side. The findings from each angle are summarized in Table 3. The analysis reveals some losses in mass flow rate, calculated as a percentage by comparing the inlet and outlet mass flow rates. At an AoA of 60°, the mass flow rate losses were measured at 0.03019%, indicating negligible errors across all simulations. Table 4 provides a comprehensive overview of the simulation results for each angle.

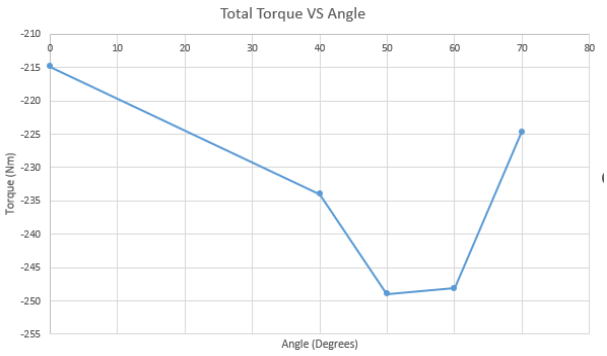

Fig. 11: Total Torque vs Angle of Attack (Baseline model)

Upon examining the trend of total torque against the angle depicted in Fig. 11, it becomes evident that the highest torque occurs at 50 degrees, registering a total torque of -248.9 Nm. Meanwhile, the simulation at 60 degrees yields a total torque of -248.1 Nm, with a relatively small difference between the two values. However, as illustrated in Fig. 6, the rotating model identifies the optimal AoA as 60 degrees. Despite the baseline model suggesting the highest torque at 50 degrees, the rotating model indicates that the highest mechanical power is achieved at 60 degrees. Therefore, misting was simulated at an Angle of Attack of 60 degrees.

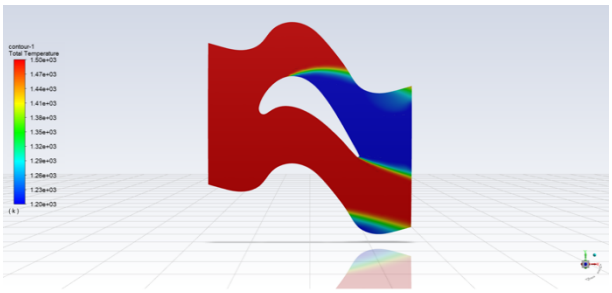

Fig. 12: Misted temperature distribution for the baseline model (AoA=60°)

Fig. 12 illustrates the temperature distribution along the body during the application of mist cooling. According to the simulation results, the temperature at the pressure side of the blade decreased to 1200 K. This successful cooling method effectively lowers the temperature, fulfilling the primary objective of the simulation, which is blade protection. Remarkably, the temperature distribution remains consistent between the rotation and non-rotation models. Additionally, it is anticipated that as the radius of the droplets increases, the heat transfer between the droplets and the blade intensifies, resulting in further temperature reduction.

Table 3: Rotating model simulation results

AoA θ (°)	Average inlet velocity (m/s)	Inlet mass flow rate (kg/s)	Torque total (Nm)	Torque suction (Nm)	Torque pressure (Nm)	Axial velocity (m/s)	Outlet mass flow rate (kg/s)	Enthalpy inlet (kJ/kg)	Enthalpy outlet (MJ/kg)	Thermodynamic energy (MJ/kg)	Thermodynamic Power (KJ/s)	Mass flow rate error (%)	Total Mechanical Power (KW)
0	259.3	1.68	-61.8	380.1	-442.7	259.3	1.7	1175.8	981.2	980.0	1642.2	0.0048	-1618.1
40	326.4	1.59	-189.7	326.8	-517.2	256.1	1.6	1153.6	1031.0	1029.9	1641.2	0.0100	-4965.0
50	385.0	1.49	-196.0	321.8	-583.3	247.5	1.5	1135.4	999.9	998.8	1490.4	0.0066	-5296.9
60	468.9	1.33	-209.1	290.2	-499.8	235.1	1.3	1099.7	996.2	995.1	1325.0	0.0029	-5472.7
70	538.4	0.98	-163.2	327.3	-490.7	184.1	0.98	1064.3	966.9	965.9	943.8	0.0054	-4271.0

Table 4: Baseline model simulation results

AoA θ (°)	Average velocity inlet (m/s)	Mass flow rate (kg/s)	Torque total (Nm)	Torque suction (Nm)	Torque pressure (Nm)	Axial velocity (m/s)	Mass flow rate out (kg/s)	Enthalpy in (kJ/kg)	Enthalpy out (kJ/kg)	Thermodynamic energy (kJ/kg)	Mass flow rate error (%)
0	262.1	1.62	-214.9	279.1	-495.1	262.1	1.62	1175.1	1042.9	132.3	0.0015
40	326.5	1.50	-234.0	313.1	-547.7	250.1	1.50	1156.1	999.4	156.7	0.0031
50	380.1	1.42	-248.9	304.3	-553.2	244.4	1.42	1136.9	977.2	159.7	0.0118
60	433.6	1.20	-248.1	316.1	-564.2	216.3	1.20	1114.4	985.7	128.7	0.0302
70	477.8	0.88	-224.7	324.5	-549.8	163.4	0.88	1094.5	1031.4	63.0	0.0003

4. Conclusion

This study simulates the flow over a turbine blade to determine the optimal Angle of Attack (AoA) and investigates the impact of an internal blade cooling method: misting. Various AoA values ranging from 40° to 70° were simulated in both rotating and stationary models. The stationary model serves as a baseline for comparison with the more realistic rotating model. Results indicate that the ideal AoA is 60°, yielding the highest total power and torque output (-5472.7 kW and -209.1 Nm, respectively) in the rotating model, a crucial aspect for gas turbines. Additionally, a total torque of -248.1 Nm was observed in the non-rotating model. After determining the ideal AoA, mist cooling was implemented to monitor its effect on temperature. Five injection points were utilized for both models, with a droplet diameter of 0.1 mm and a droplet temperature of 300 K. The mass flow rate of the droplets was set to 0.1% of the air's flow rate (0.00133 kg/s for the rotating model). Results demonstrate the success of the cooling method, with temperatures on various blade areas decreasing from 1500 K to 1200 K in both models. Furthermore, it is recommended to use a smaller interval for future AoA investigations and to increase the diameter of droplets and the number of injection points for misting. This adjustment would enhance heat transfer efficiency between the blade and the droplet, thereby improving mist cooling effectiveness.

Nomenclature

P	Pressure, bar
T	Temperature, K
h	Enthalpy, J/kg
L	Length, m
t	Time, s
$\dot{m}$	Mass flow rate, Kg/s
V	Flow Velocity, m/s
W	Relative velocity, m/s
U	Tangential Velocity, m/s
P_s	Shaft power, W
g	Gravity, m/s^2

Greek Symbols

μ	Dynamic viscosity, Pa s
ρ	Mass density, kg/m^3
θ	Angle, degrees
ω	Rotation Speed, rpm

Subscripts

x	x-component
y	y-component
z	z-component
i	index
j	index
in	inlet
out	outlet
H	high
L	Low
u	Tangential

Notations

$\frac{\partial y}{\partial x}$	Partial derivative

Non-dimensional Numbers

Re	Reynolds number

References

[1] J. E. Shaw, "Comparing Carnot, Stirling, otto, brayton and diesel cycles," *Transactions of the Missouri Academy of Science*, vol. 42, no. 2008, pp. 1–6, 2008, doi: 10.30956/0544- 540x-42.2008.1.

[2] U. Ali and M. S. Kamran, "Geometric optimization of a gas turbine blade cooling passage using CFD,"

International Journal of Thermal and Environmental Engineering, vol. 17, no. 02, 2020, doi: 10.5383/ijtee.17.02.004.

[3] M. R. Reyhani, M. Alizadeh, A. Fathi, and H. Khaledi, "Turbine blade temperature calculation and life estimation - A sensitivity analysis," Propulsion and Power Research, vol. 2, no. 2, pp. 148–161, Jun. 2013. doi: 10.1016/j.jppr.2013.04.004.

[4] S. Abed, T. Khir, and A. Ben Brahim, "Thermodynamic and energy study of a regenerator in gas turbine cycle and optimization of performances," *International Journal of Energy Optimization and Engineering*, vol. 5, no. 2, pp. 25–44, 2016, doi: 10.1109/irec.2014.6826920.

[5] X. Li and T. Wang, "Simulation of film cooling enhancement with mist injection," Volume 3: Turbo Expo 2005, Parts A and B, 2005.

[6] T. Wang and X. Li, "Simulation of mist film cooling at gas turbine operating conditions," Volume 3: Heat Transfer, Parts A and B, 2006.

[7] T. S. Dhanasekaran and T. Wang, "Simulation of mist film cooling on rotating gas turbine blades," Journal of Heat Transfer, vol. 134, no. 1, Oct. 2011. doi:10.1115/1.4004480

[8] Y. Jiang et al., "Conjugate heat transfer simulation of turbine blade high efficiency cooling method with mist injection," Proceedings of the Institution of Mechanical Engineers, Part C: Journal of Mechanical Engineering Science, vol. 228, no. 15, pp. 2738–2749, Feb. 2014. doi:10.1177/0954406214522436

[9] R. K. Bhargava, C. B. Meher-Homji, M. A. Chaker, M. Bianchi, F. Melino, A. Peretto, and S. Ingistov, "Gas turbine fogging technology — a state-of-the-art review: Part III — practical considerations and operational experience," Volume 4: Turbo Expo 2005, 2005.

[10] M. Chaker, C. B. Meher-Homji, and T. Mee, "Inlet fogging of gas turbine engines: Part B — fog droplet sizing analysis, nozzle types, measurement and testing," Volume 4: Turbo Expo 2002, Parts A and B, 2002.

[11] W. Z. Shen, M. O. Hansen, and J. N. Sørensen, "Determination of the angle of attack on rotor blades," Wind Energy, vol. 12, no. 1, pp. 91–98, 2009.

[12] S. Barakat, A. Ramzy, A. M. Hamed, and S. H. El-Emam, "Augmentation of gas turbine performance using integrated EAHE and Fogging Inlet Air Cooling System," Energy, vol. 189, p. 116133, Dec. 2019. doi: 10.1016/j.energy.2019.11613.

[13] A. Sohani, Y. Farasati, and H. Sayyaadi, "A systematic approach to find the Best Road Map for enhancement of a power plant with dew point inlet air pre-cooling of the Air Compressor," Energy Conversion and Management, vol. 150, pp. 463–484, Oct. 2017. doi: 10.1016/j.enconman.2017.08.028.

[14] A. K. Shukla and O. Singh, "Thermodynamic investigation of parameters affecting the execution of steam injected cooled gas turbine based combined cycle power plant with vapor absorption inlet air cooling," Applied Thermal Engineering, vol. 122, pp. 380–388, Jul. 2017. doi: 10.1016/j.applthermaleng.2017.05.034.

[15] U. Ali, O. Al-Mufti, and I. Janajreh, "Harnessing sound waves for sustainable energy: Advancements and challenges in thermoacoustic technology," Energy Nexus, vol. 15, p. 100320, Sep. 2024, doi: 10.1016/j.nexus.2024.100320.

[16] G. Barigozzi, A. Perdichizzi, C. Gritti, and I. Guaiatelli, "Techno-economic analysis of gas turbine inlet air cooling for combined cycle power plant for different climatic conditions" Applied Thermal Engineering, vol. 82, pp. 57–67, May 2015. doi: 10.1016/j.applthermaleng.2015.02.049.

[17] A. Simpson, S. W. Spence, D. W. Artt, and G. McCullough, "Experimental and numerical investigation of varying stator design parameters for a radial turbine," Volume 6: Turbomachinery, Parts A and B, 2006.